

**UNITED STATES AIR FORCE
ARMSTRONG LABORATORY**

**Three-Dimensional Electromagnetic
Scattering From Arbitrary
Inhomogeneous Objects**

Sherwood Samn

January 1997

19970515 075

*Approved for public release;
distribution is unlimited.*

**Occupational and Environmental Health
Directorate
Mathematical Products Division
2503 Gillingham Dr.
Brooks AFB, TX 78235-5102**

DTIC QUALITY INSPECTED 1

NOTICES

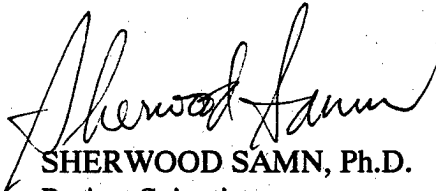
When Government drawings, specifications, or other data are used for any purpose other than in connection with a definitely Government-related procurement, the United States Government incurs no responsibility or any obligation whatsoever. The fact that the Government may have formulated or in any way supplied the said drawings, specifications, or other data, is not to be regarded by implication, or otherwise in any manner construed, as licensing the holder or any other person or corporation; or as conveying any rights or permission to manufacture, use, or sell any patented invention that may in any way be related thereto.

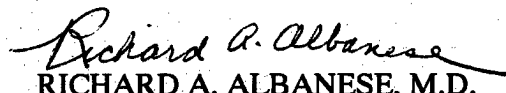
The Office of Public Affairs has reviewed this report, and it is releasable to the National Technical Information Service, where it will be available to the general public, including foreign nationals.

This report has been reviewed and is approved for publication.

Government agencies and their contractors registered with Defense Technical Information Center (DTIC) should direct requests for copies to: Defense Technical Information Center, 8725 John J. Kingman Rd., STE 0944, Ft. Belvoir, VA 22060-6218.

Non-Government agencies may purchase copies of this report from: National Technical Information Services (NTIS), 5285 Port Royal Road, Springfield, VA 22161-2103.


SHERWOOD SAMN, Ph.D.
Project Scientist


RICHARD A. ALBANESE, M.D.
Chief, Mathematical Products
Division

REPORT DOCUMENTATION PAGE			Form Approved OMB No. 0704-0188	
Public reporting burden for this collection of information is estimated to average 1 hour per response, including the time for reviewing instructions, searching existing data sources, gathering and maintaining the data needed, and completing and reviewing the collection of information. Send comments regarding this burden estimate or any other aspect of this collection of information, including suggestions for reducing this burden, to Washington Headquarters Services, Directorate for Information Operations and Reports, 1215 Jefferson Davis Highway, Suite 1204, Arlington, VA 22202-4302, and to the Office of Management and Budget, Paperwork Reduction Project (0704-0188), Washington, DC 20503.				
1. AGENCY USE ONLY (Leave blank)		2. REPORT DATE January 1997		3. REPORT TYPE AND DATES COVERED Interim Jun 95 - Mar 96
4. TITLE AND SUBTITLE Three-Dimensional Electromagnetic Scattering from Arbitray Inhomogeneous Objects			5. FUNDING NUMBERS PE-62202F PR-7757 TA-B4 WU-02	
6. AUTHOR(S) Sherwood Samn				
7. PERFORMING ORGANIZATION NAME(S) AND ADDRESS(ES) Armstrong Laboratory (AFMC) Occupational and Environmental Health Directorate Mathematical Products Division 2503 Gillingham Dr., Bldg 175E Brooks Air Force Base, TX 78235-5102			8. PERFORMING ORGANIZATION REPORT NUMBER AL/OE-TR-1997-0021	
9. SPONSORING/MONITORING AGENCY NAME(S) AND ADDRESS(ES) Armstrong Laboratory (AFMC) Occupational and Environmental Health Directorate Mathematical Products Division 2503 Gillingham Dr., Bldg 175E Brooks Air Force Base, TX 78235-5102			10. SPONSORING/MONITORING AGENCY REPORT NUMBER	
11. SUPPLEMENTARY NOTES				
12a. DISTRIBUTION AVAILABILITY STATEMENT Approved for public release; distribution is unlimited			12b. DISTRIBUTION CODE	
13. ABSTRACT (Maximum 200 words) For microwave dosimetry an accurate mathematical model of interior scattering is needed. An integral equation approach using the Moment Method with Whitney basis functions is adopted. This interim report describes the mathematical formulation of lthe problem, and some validation results for a sphere.				
14. SUBJECT TERMS Electromagnetics, Moment Method, Whitmely Basis Functions, Integral Equation, Mie Solution, Dyadic Green Function			15. NUMBER OF PAGES	
			16. PRICE CODE	
17. SECURITY CLASSIFICATION OF REPORT Unclassified	18. SECURITY CLASSIFICATION OF THIS PAGE Unclassified	19. SECURITY CLASSIFICATION OF ABSTRACT UnclassifiedUL	20. LIMITATION OF ABSTRACT	

TABLE OF CONTENTS

	<u>Page</u>
INTRODUCTION	1
DERIVATION OF MODEL EQUATIONS	1
SINGULARITY OF THE DYADIC GREEN'S FUNCTION	5
SOLUTION METHOD	8
EDGE-BASED VECTOR BASIS FUNCTIONS	10
EVALUATION OF U_n	12
RESULTS	14
DISCUSSION	16
CONCLUSION	17
REFERENCES	18

FIGURES

<u>Figure No.</u>	<u>Page</u>
1. Discretization (D1) of a Sphere	21
2. Discretization (D1) of a Sphere (Shrunk)	22
3. Tetrahedron Volume Distribution (D1)	23
4. Discretization (D2) of a Sphere	24
5. Discretization (D2) of a Sphere (Shrunk)	25
6. Tetrahedron Volume Distribution (D2)	26
7. Preferred Discretization of a Sphere	27
8. Preferred Discretization of a Sphere (Shrunk)	28
9. Tetrahedron Volume Distribution (Preferred)	29
10. Transparent Case	30
11. Translucent Case: 120 Tetrahedra	31
12. Translucent Case: 400 Tetrahedra	32
13. Sensitivity: Relative Permittivity	33
14. Sensitivity: Frequency	34

THREE-DIMENSIONAL ELECTROMAGNETIC SCATTERING FROM ARBITRARY INHOMOGENEOUS OBJECTS

Introduction

The purpose of this paper is to describe the work we have done towards developing a versatile and efficient method for calculating electromagnetic energy deposition in arbitrary three-dimensional inhomogeneous objects.

Given an incident field \mathbf{E}^{inc} generated from, for example, an antenna, the problem is to estimate the amount of electromagnetic energy deposition in a nearby human object. While this is a classical problem, a versatile and efficient method for solving it in realistic settings is not generally available [10]. Some recent research in this area can be found in [24, 25, 26] and their references. Understanding the details of electromagnetic deposition in humans is essential for health and safety exposure considerations. Knowledge of deposition in humans and non-human animals is very important to medical research on the bioeffects of radiation exposure.

Derivation of Model Equations

The stated problem involves solving the symmetric Maxwell's equations:

$$\begin{aligned}\nabla \times \tilde{\mathbf{E}} &= -\frac{\partial \tilde{\mathbf{B}}}{\partial t} - \tilde{\mathbf{J}}_m^{fict} \\ \nabla \times \tilde{\mathbf{H}} &= \frac{\partial \tilde{\mathbf{D}}}{\partial t} + \tilde{\mathbf{J}}^{true} \\ \nabla \cdot \tilde{\mathbf{D}} &= \tilde{\rho}^{true} \\ \nabla \cdot \tilde{\mathbf{B}} &= \tilde{\rho}_m^{fict}\end{aligned}$$

for the electric and magnetic field intensities $\tilde{\mathbf{E}}$ and $\tilde{\mathbf{H}}$, and the electric and magnetic flux densities $\tilde{\mathbf{D}}$ and $\tilde{\mathbf{B}}$ everywhere in \mathbf{R}^3 including the object. We assume the body (scatterer) occupies a bounded region V in free space. Here the electric sources $\tilde{\rho}^{true}$ and $\tilde{\mathbf{J}}^{true}$ are respectively the charge and current

densities. For the sake of symmetry, the fictitious and identically vanishing magnetic sources $\tilde{\rho}_m^{fict}$ and $\tilde{\mathbf{J}}_m^{fict}$ are introduced. All dependent (“tilded”) variables are assumed to be functions of space and time.

We assume the object is linear, isotropic and nondispersive. Then

$$\begin{aligned}\tilde{\mathbf{D}} &= \varepsilon \tilde{\mathbf{E}} \\ \tilde{\mathbf{B}} &= \mu \tilde{\mathbf{H}} \\ \tilde{\mathbf{J}}^{true} &= \sigma \tilde{\mathbf{E}}\end{aligned}$$

where ε , μ , and σ , all possibly spatially-dependent, are respectively the permittivity, the permeability, and the conductivity of the body. Outside the body, the first two of these equations hold with the constant free-space parameters ε_0 and μ_0 respectively.

If we let $\mu(\mathbf{r}) = \mu_0 + \delta\mu(\mathbf{r})$ and $\varepsilon(\mathbf{r}) = \varepsilon_0 + \delta\varepsilon(\mathbf{r})$, where $\mathbf{r} = (x, y, z)$, then the Maxwell’s equations can be written as

$$\begin{aligned}\nabla \times \tilde{\mathbf{E}} &= -\mu_0 \frac{\partial \tilde{\mathbf{H}}}{\partial t} - \tilde{\mathbf{J}}_m \\ \nabla \times \tilde{\mathbf{H}} &= \varepsilon_0 \frac{\partial \tilde{\mathbf{E}}}{\partial t} + \tilde{\mathbf{J}} \\ \nabla \cdot \tilde{\mathbf{E}} &= \tilde{\rho} / \varepsilon_0 \\ \nabla \cdot \tilde{\mathbf{H}} &= \tilde{\rho}_m / \mu_0\end{aligned}$$

where

$$\begin{aligned}\tilde{\mathbf{J}}_m &= \delta\mu \frac{\partial \tilde{\mathbf{H}}}{\partial t} + \tilde{\mathbf{J}}_m^{fict} \\ \tilde{\mathbf{J}} &= \delta\varepsilon \frac{\partial \tilde{\mathbf{E}}}{\partial t} + \tilde{\mathbf{J}}^{true} \\ \tilde{\rho} &= \tilde{\rho}^{true} - \nabla \cdot \delta\varepsilon \tilde{\mathbf{E}} \\ \tilde{\rho}_m &= \tilde{\rho}_m^{fict} - \nabla \cdot \delta\mu \tilde{\mathbf{H}}\end{aligned}$$

If we further assume the sources vary sinusoidally with time, then the problem reduces to solving the time-harmonic equations:

$$\nabla \times \mathbf{E} = -j\beta\omega\mu_0\mathbf{H} - \mathbf{J}_m \quad (1)$$

$$\nabla \times \mathbf{H} = j\beta\omega\varepsilon_0\mathbf{E} + \mathbf{J} \quad (2)$$

$$\nabla \cdot \mathbf{E} = \rho / \varepsilon_0 \quad (3)$$

$$\nabla \cdot \mathbf{H} = \rho_m / \mu_0 \quad (4)$$

subject to appropriate boundary conditions on the \mathbf{E} and \mathbf{H} fields. Here the phasor \mathbf{E} is related to $\tilde{\mathbf{E}}$ by the equation

$$\tilde{\mathbf{E}}(x, y, z, t) = \Re[\mathbf{E}(x, y, z)e^{j\beta\omega t}]$$

where $\beta = \pm 1$. Similarly, the same can be said for the other dependent variables. Clearly, we must have

$$\mathbf{J}_m = j\beta\omega\delta\mu\mathbf{H} + \mathbf{J}_m^{fict} \quad (5)$$

$$\mathbf{J} = j\beta\omega\delta\epsilon\mathbf{E} + \mathbf{J}^{true} \quad (6)$$

$$\rho = \rho^{true} - \nabla \cdot \delta\epsilon\mathbf{E} \quad (7)$$

$$\rho_m = \rho_m^{fict} - \nabla \cdot \delta\mu\mathbf{H} \quad (8)$$

If the electric and magnetic intensities \mathbf{E} and \mathbf{H} satisfy the time harmonic equations, Equations (1)-(4), then

$$\nabla \cdot \mathbf{J} = -j\beta\omega\rho \quad (9)$$

$$\nabla \cdot \mathbf{J}_m = -j\beta\omega\rho_m \quad (10)$$

Or, equivalently, in terms of the original variables,

$$\nabla \cdot \mathbf{J}^{true} = -j\beta\omega\rho^{true} \quad (11)$$

$$\nabla \cdot \mathbf{J}_m^{fict} = -j\beta\omega\rho_m^{fict} \quad (12)$$

These are the equations of continuity. Conversely, if \mathbf{E} and \mathbf{H} satisfy Equations (1) and (2), then Equations (3) and (4) are automatically satisfied, provided the equation of continuity for the electric sources \mathbf{J}^{true} and ρ^{true} holds. Since we will always assume this to be true, it suffices to solve only Equations (1) and (2).

Taking the “curl” of Equation (1) and then substituting Equation (2) in the result, we obtain the equation

$$\nabla \times \nabla \times \mathbf{E} - \omega^2\epsilon_o\mu_o\mathbf{E} = -j\beta\omega\mu_o\mathbf{J} - \nabla \times \mathbf{J}_m \quad (13)$$

The formulation up to this point has been quite general. However, we will now make the simplifying assumptions that $\mu = \mu_o$ everywhere inside the

body. It follows that $\mathbf{J}_m = \mathbf{0}$ and $\rho_m = 0$ everywhere, as \mathbf{J}_m^{fict} and ρ_m^{fict} vanish identically in reality. Thus, Equation (13) simplifies to

$$\nabla \times \nabla \times \mathbf{E} - k_o^2 \mathbf{E} = -j\beta\omega\mu_o \mathbf{J} \quad (14)$$

where

$$k_o^2 = \omega^2 \epsilon_o \mu_o$$

If we let $\bar{\mathbf{G}}(\mathbf{r}, \mathbf{r}')$ denote the free-space Dyadic Green's Function, so that

$$\bar{\mathbf{G}}(\mathbf{r}, \mathbf{r}') = (\bar{\mathbf{I}} + \frac{1}{k_o^2} \nabla \nabla) g(\mathbf{r}, \mathbf{r}')$$

where

$$g(\mathbf{r}, \mathbf{r}') = \frac{e^{-j\beta k_o |\mathbf{r} - \mathbf{r}'|}}{4\pi |\mathbf{r} - \mathbf{r}'|}$$

is the Green's function for the three-dimensional scalar Helmholtz equation, then, treating the right-hand-side of Equation (14) as a source (even though it contains the unknown field \mathbf{E} through the definition of \mathbf{J}), it can be shown that the electric field \mathbf{E} formally satisfies the following Fredholm integral equation (of the second kind):

$$\begin{aligned} \mathbf{E}(\mathbf{r}) &= -j\beta\omega\mu_o \int_{V \cup V_J^c} \bar{\mathbf{G}}(\mathbf{r}, \mathbf{r}') \cdot \mathbf{J}(\mathbf{r}') d\mathbf{r}' \\ &= -j\beta\omega\mu_o \int_{V \cup V_J^c} \bar{\mathbf{G}}(\mathbf{r}, \mathbf{r}') \cdot [j\beta\omega\delta\epsilon(\mathbf{r}') \mathbf{E}(\mathbf{r}') + \mathbf{J}^{true}(\mathbf{r}')] d\mathbf{r}' \\ &= -j\beta\omega\mu_o \int_V \bar{\mathbf{G}}(\mathbf{r}, \mathbf{r}') \cdot [j\beta\omega\delta\epsilon(\mathbf{r}') \mathbf{E}(\mathbf{r}') + \mathbf{J}^{true}(\mathbf{r}')] d\mathbf{r}' \\ &\quad -j\beta\omega\mu_o \int_{V_J^c} \bar{\mathbf{G}}(\mathbf{r}, \mathbf{r}') \cdot \mathbf{J}^{true}(\mathbf{r}') d\mathbf{r}' \end{aligned}$$

where V_J^c denotes that region in space outside the body V where the "source" \mathbf{J} does not vanish. Here, we have used the fact that $\delta\epsilon = 0$ in V^c , the region external to V . Since we are assuming the body medium is linear, so that $\mathbf{J}^{true}(\mathbf{r}) = \sigma(\mathbf{r}) \mathbf{E}(\mathbf{r})$, it follows that

$$\begin{aligned} \mathbf{E}(\mathbf{r}) &= \omega^2 \mu_o \int_V \bar{\mathbf{G}}(\mathbf{r}, \mathbf{r}') \cdot [\tau(\mathbf{r}') \mathbf{E}(\mathbf{r}')] d\mathbf{r}' \\ &\quad -j\beta\omega\mu_o \int_{V_J^c} \bar{\mathbf{G}}(\mathbf{r}, \mathbf{r}') \cdot \mathbf{J}^{true}(\mathbf{r}') d\mathbf{r}' \end{aligned} \quad (15)$$

where

$$\tau(\mathbf{r}) = \delta\epsilon(\mathbf{r}) - \frac{j\beta\sigma(\mathbf{r})}{\omega}$$

Since the electric field \mathbf{E} is identical to the incident field \mathbf{E}^{inc} when there is no scatterer ($\delta\epsilon = 0$ and $\sigma = 0$), the last integral in Equation (15) must be the incident field:

$$\mathbf{E}^{inc}(\mathbf{r}) = -j\beta\omega\mu_o \int_{V_s^c} \bar{G}(\mathbf{r}, \mathbf{r}') \cdot \mathbf{J}^{true}(\mathbf{r}') d\mathbf{r}'$$

Thus, the model (integral) equation we need to solve is:

$$\mathbf{E}(\mathbf{r}) + \beta_o \int_V \bar{G}(\mathbf{r}, \mathbf{r}') \cdot [\tau(\mathbf{r}') \mathbf{E}(\mathbf{r}')] d\mathbf{r}' = \mathbf{E}^{inc}(\mathbf{r}) \quad (16)$$

where

$$\beta_o = -\omega^2\mu_o$$

Singularity of the Dyadic Green's Function

At each field point \mathbf{r} inside the region V , the model equation, Equation (16), becomes singular, since $\bar{G}(\mathbf{r}, \mathbf{r}')$ is undefined when the source point \mathbf{r}' coincides with the field point \mathbf{r} .

The singularity of the Dyadic Green's Function has been well-studied ([17],[18], [15], [20]). The singular integral in Equation (16) can be handled "as usual" as follows.

$$\begin{aligned} \int_V \bar{G}(\mathbf{r}, \mathbf{r}') \cdot [\tau(\mathbf{r}') \mathbf{E}(\mathbf{r}')] d\mathbf{r}' &= \lim_{|V_s| \rightarrow 0} \left(\int_{V-V_s} \bar{G}(\mathbf{r}, \mathbf{r}') \cdot [\tau(\mathbf{r}') \mathbf{E}(\mathbf{r}')] d\mathbf{r}' + \right. \\ &\quad \left. \int_{V_s} \bar{G}(\mathbf{r}, \mathbf{r}') \cdot [\tau(\mathbf{r}') \mathbf{E}(\mathbf{r}')] d\mathbf{r}' \right) \end{aligned} \quad (17)$$

where V_s are ever-shrinking volumes surrounding the field point \mathbf{r} . However, what is unusual about this approach is the fact that the limiting process is not uniform. In particular, the limiting values of the two integrals on the right will generally be different, depending on the shapes of V_s . Nevertheless, the sum of the two will always be the same.

If the V_s are chosen to be spheres, then it can be shown ([17], [15],[20], [7]) that

$$\lim_{|V_s| \rightarrow 0} \int_{V_s} \bar{G}(\mathbf{r}, \mathbf{r}') \cdot [\tau(\mathbf{r}') \mathbf{E}(\mathbf{r}')] d\mathbf{r}' = -\frac{\tau(\mathbf{r}) \mathbf{E}(\mathbf{r})}{3k_o^2} \quad (18)$$

Thus, Equation (16) becomes

$$\alpha_o(\mathbf{r})\mathbf{E}(\mathbf{r}) + \beta_o \mathbf{U}_{pv}(\mathbf{r}) = \mathbf{E}^{inc}(\mathbf{r}) \quad (19)$$

where

$$\alpha_o(\mathbf{r}) = 1 + \frac{\tau(\mathbf{r})}{3\epsilon_o} \quad (20)$$

and

$$\mathbf{U}_{pv}(\mathbf{r}) = \text{PV} \int_V \bar{G}(\mathbf{r}, \mathbf{r}') \cdot [\tau(\mathbf{r}') \mathbf{E}(\mathbf{r}')] d\mathbf{r}' \quad (21)$$

Here PV stands for principal value integration (using shrinking spheres). This formulation has been employed by Livesay and Chen [12] and many other researchers ([5], [18], [4]).

The principal value integration in Equation (19) generally cannot be evaluated, analytically or numerically. An equivalent but more practical approach is to re-formulate the singular integral in Equation (17). Defining

$$\mathbf{F}(\mathbf{r}) = \tau(\mathbf{r}) \mathbf{E}(\mathbf{r}),$$

and using a representation of $\mathbf{E}(\mathbf{r})$ that involves vector and scalar potentials, one can replace this singular integral by

$$\mathbf{U}_{fn}(\mathbf{r}) \equiv (\bar{\mathbf{I}} + \frac{1}{k_o^2} \nabla \nabla) \cdot \int_V g(\mathbf{r}, \mathbf{r}') \mathbf{F}(\mathbf{r}') d\mathbf{r}'$$

Moreover, $\mathbf{U}_{fn}(\mathbf{r})$ can be expressed, without principal value integration, as ([8, 11, 19, 20])

$$\mathbf{U}_{fn}(\mathbf{r}) = \mathbf{I}_1(\mathbf{r}) + \mathbf{I}_2(\mathbf{r}) + \mathbf{I}_3(\mathbf{r}) \quad (22)$$

where

$$\begin{aligned} \mathbf{I}_1(\mathbf{r}) &= \int_{V-V_T} \bar{G}(\mathbf{r}, \mathbf{r}') \cdot \mathbf{F}(\mathbf{r}') d\mathbf{r}' \\ \mathbf{I}_2(\mathbf{r}) &= \int_{V_T} \bar{G}(\mathbf{r}, \mathbf{r}') \cdot \mathbf{F}(\mathbf{r}') - \bar{G}_o(\mathbf{r}, \mathbf{r}') \cdot \mathbf{F}(\mathbf{r}) d\mathbf{r}' \\ \mathbf{I}_3(\mathbf{r}) &= \frac{1}{k_o^2} \int_{S_T} \frac{\hat{\mathbf{n}}(\mathbf{r}') (\mathbf{r} - \mathbf{r}')}{4\pi |\mathbf{r} - \mathbf{r}'|^3} \cdot \mathbf{F}(\mathbf{r}) dS' \end{aligned}$$

Here, the region V_T is any finite (not necessarily infinitesimal) region enclosing \mathbf{r} and is contained in V . S_T is the surface area of V_T . The outward normal of S_T at a point \mathbf{r}' on S_T is denoted by $\hat{\mathbf{n}}(\mathbf{r}')$. Finally, \bar{G}_o is the so-called static Dyadic Green's Function defined by

$$\bar{G}_o(\mathbf{r}, \mathbf{r}') = \frac{1}{k_o^2} \nabla \nabla g_o(\mathbf{r}, \mathbf{r}')$$

where

$$g_o(\mathbf{r}, \mathbf{r}') = \frac{1}{4\pi |\mathbf{r} - \mathbf{r}'|}$$

In their derivation of the representation above, Fikioris [8], Lee [11], and Wang ([19], [20]) require \mathbf{F} to satisfy a Hölder condition. \mathbf{F} satisfies a Hölder condition at a point \mathbf{r} if there are three positive constants A, B , and C such that

$$|\mathbf{F}(\mathbf{r}) - \mathbf{F}(\mathbf{r}')| \leq A |\mathbf{r} - \mathbf{r}'|^B$$

for all \mathbf{r}' satisfying $|\mathbf{r} - \mathbf{r}'| \leq C$

It is interesting to note that

$$\begin{aligned} \text{PV} \int_{V_T} \bar{G}_o(\mathbf{r}, \mathbf{r}') \cdot \mathbf{F}(\mathbf{r}) \, d\mathbf{r}' &\neq \frac{1}{k_o^2} \int_{S_T} \hat{\mathbf{n}}(\mathbf{r}') \nabla' g_o(\mathbf{r}, \mathbf{r}') \, dS' \cdot \mathbf{F}(\mathbf{r}) \\ &= \frac{1}{k_o^2} \int_{S_T} \frac{\hat{\mathbf{n}}(\mathbf{r}') (\mathbf{r} - \mathbf{r}')}{4\pi |\mathbf{r} - \mathbf{r}'|^3} \, dS' \cdot \mathbf{F}(\mathbf{r}) \\ &= \mathbf{I}_3(\mathbf{r}) \end{aligned}$$

This can be verified, for example, by assuming V_T is a sphere centered at \mathbf{r} . For in this case,

$$\text{PV} \int_{V_T} \bar{G}_o(\mathbf{r}, \mathbf{r}') \cdot \mathbf{F}(\mathbf{r}) \, d\mathbf{r}' = \mathbf{0}$$

but

$$\frac{1}{k_o^2} \int_{S_T} \frac{\hat{\mathbf{n}}(\mathbf{r}') (\mathbf{r} - \mathbf{r}')}{4\pi |\mathbf{r} - \mathbf{r}'|^3} \, dS' \cdot \mathbf{F}(\mathbf{r}) = -\frac{1}{3k_o^2} \mathbf{F}(\mathbf{r}) = \mathbf{I}_3(\mathbf{r})$$

Consequently,

$$\begin{aligned} \mathbf{U}_{\text{fn}}(\mathbf{r}) &\neq \int_{V-V_T} \bar{G}(\mathbf{r}, \mathbf{r}') \cdot \mathbf{F}(\mathbf{r}') \, d\mathbf{r}' + \text{PV} \int_{V_T} \bar{G}(\mathbf{r}, \mathbf{r}') \cdot \mathbf{F}(\mathbf{r}') \, d\mathbf{r}' \\ &= \text{PV} \int_V \bar{G}(\mathbf{r}, \mathbf{r}') \cdot \mathbf{F}(\mathbf{r}') \, d\mathbf{r}' \end{aligned}$$

This implies that the relationship

$$(\bar{\mathbf{I}} + \frac{1}{k_o^2} \nabla \nabla) \cdot \int_V g(\mathbf{r}, \mathbf{r}') \mathbf{F}(\mathbf{r}') d\mathbf{r}' = PV \int_V (\bar{\mathbf{I}} + \frac{1}{k_o^2} \nabla \nabla) \cdot g(\mathbf{r}, \mathbf{r}') \mathbf{F}(\mathbf{r}') d\mathbf{r}' \quad (23)$$

is at best formal. The left side of Equation (23) is the correct term to use, though it is numerically undesirable. Its equivalent three-term form in Equation (22), while more complicated, is numerically better behaved. Finally, the right side of Equation (23) is incompletely defined, requiring additional qualifications (principal volume being used and its associated correction term) for its correctness.

One can also show in the special case in which V_T is a sphere that \mathbf{I}_2 will approach zero as the radius of the sphere approaches zero, so that a result implicit in Equation (19) is recovered:

$$(\bar{\mathbf{I}} + \frac{1}{k_o^2} \nabla \nabla) \cdot \int_V g(\mathbf{r}, \mathbf{r}') \mathbf{F}(\mathbf{r}') d\mathbf{r}' = PV \int_V \bar{G}(\mathbf{r}, \mathbf{r}') \cdot \mathbf{F}(\mathbf{r}') d\mathbf{r}' - \frac{1}{3k_o^2} \mathbf{F}(\mathbf{r}) \quad (24)$$

Or, equivalently,

$$\mathbf{U}_{fn}(\mathbf{r}) = \mathbf{U}_{pv}(\mathbf{r}) - \frac{1}{3k_o^2} \mathbf{F}(\mathbf{r})$$

In short, using the representation of the singular integral given in Equation (22), we obtain an alternate representation of the model equation given in (19) but which does not require making a principal volume integration:

$$\mathbf{E}(\mathbf{r}) + \beta_o \mathbf{U}_{fn}(\mathbf{r}) = \mathbf{E}^{inc}(\mathbf{r}) \quad (25)$$

This has exactly the same form as Equation (16) except the integral is now unambiguously defined.

Solution Method

To solve the integral equation (19) or its alternate form in equation (25), we use the classical Moment Method (MM) [9]. In this report, we will concentrate on solving equation (19). Because we do not assume the scatterer to be homogeneous, $\mathbf{E}(\mathbf{r})$ is generally not divergence-free. (See Equations (3) and (7).) As we will see in the next section, it is consistent with our approach

if the field being sought is divergence-free. Thus, instead of applying MM to equation (19), we will apply it to the following equivalent integral equation:

$$\alpha_1(\mathbf{r})\hat{\mathbf{E}}(\mathbf{r}) + \beta_o \text{PV} \int_V \bar{\mathbf{G}}(\mathbf{r}, \mathbf{r}') \cdot [\tau_1(\mathbf{r}') \hat{\mathbf{E}}(\mathbf{r}')] d\mathbf{r}' = \mathbf{E}^{inc}(\mathbf{r}) \quad (26)$$

where

$$\begin{aligned} \alpha_1(\mathbf{r}) &= \alpha_0(\mathbf{r}) \hat{\alpha}_1(\mathbf{r}) \\ \hat{\alpha}_1(\mathbf{r}) &= \frac{\epsilon_o}{\epsilon_o + \tau(\mathbf{r})} \\ \tau_1(\mathbf{r}) &= \hat{\alpha}_1(\mathbf{r}) \tau(\mathbf{r}) \\ \hat{\mathbf{E}}(\mathbf{r}) &= \mathbf{E}(\mathbf{r}) / \hat{\alpha}_1(\mathbf{r}) \end{aligned}$$

Clearly, $\hat{\alpha}_1(\mathbf{r})\hat{\mathbf{E}}(\mathbf{r}) = \mathbf{E}(\mathbf{r})$ and $\tau_1(\mathbf{r})\hat{\mathbf{E}}(\mathbf{r}) = \tau(\mathbf{r})\mathbf{E}(\mathbf{r}) = \mathbf{F}(\mathbf{r})$. More importantly, it can readily be verified that $\hat{\mathbf{E}}$ is now divergence-free ($\nabla \cdot \hat{\mathbf{E}} = 0$.)

In MM, the unknown field $\hat{\mathbf{E}}$ is assumed to be expandable in a family of basis functions $\{\mathbf{f}_n\}$:

$$\hat{\mathbf{E}}(\mathbf{r}) = \sum_{n=1}^N a_n \mathbf{f}_n(\mathbf{r}) \quad (27)$$

where $\{a_n\}_{n=1}^N$ are complex constants to be determined. When Equation (27) is substituted into Equation (26), we readily obtain

$$\sum_{n=1}^N a_n \{ \alpha_1(\mathbf{r}) \mathbf{f}_n(\mathbf{r}) + \beta_o \mathbf{U}_n(\mathbf{r}) \} = \mathbf{E}^{inc}(\mathbf{r}) \quad (28)$$

where

$$\mathbf{U}_n(\mathbf{r}) = \text{PV} \int_V \bar{\mathbf{G}}(\mathbf{r}, \mathbf{r}') \cdot [\tau_1(\mathbf{r}') \mathbf{f}_n(\mathbf{r}')] d\mathbf{r}' \quad (29)$$

Starting with Equation (28), there are two common methods to determine the N complex constants $\{a_n\}_{n=1}^N$. One can evaluate Equation (28) at N distinct points, $\mathbf{r} = \mathbf{r}_i, i = 1, \dots, N$, to obtain a system of N linear equations in N unknowns. This is the so-called point-matching method. Alternately, we can integrate Equation (28) with each of the N basis functions \mathbf{f}_n in turn to get again a system of N linear equations in N unknowns. This is the so-called Galerkin's Method. This is the method we have used in this study. The optimality of the Galerkin's Method has recently been discussed in [21].

Two issues remains to be addressed to complete the description of the solution method. One is the choice of basis functions $\{\mathbf{f}_n\}$ and the other is a method to evaluate the integral defining $\mathbf{U}_n(\mathbf{r})$ in Equation (29).

Edge-based vector basis functions

All numerical solutions are approximations of the exact solutions. Thus, even though exact solutions to Equations (1, 2) will automatically satisfy Equations (3, 4) in light of the Equations of Continuity, Equations (11,12), numerical solutions to Equations (1, 2) may be far from satisfying Equation (11).

The requirement that Equation (3) be satisfied can readily be shown to be equivalent to the condition $\nabla \cdot \hat{\mathbf{E}} = 0$. Since

$$\hat{\mathbf{E}}(\mathbf{r}) = \sum_{n=1}^N a_n \mathbf{f}_n(\mathbf{r}),$$

this condition is automatically satisfied if $\nabla \cdot \mathbf{f}_n = 0$ for each \mathbf{f}_n . In finite element methods, a well-known class of functions with this property is the class of Whitney functions of degree 1 ([23], [3]). We adopt this family for our use here. For sake of completeness, we will define this family and mention some of its properties relevant to our numerical procedure.

In the numerical solution of Equation (19), we approximate the region V occupied by the body by a family of N_t disjoint tetrahedra $\{T_i\}_{i=1}^{N_t}$. Since there are six edges to a tetrahedron, there will be a large number, say N_e , of edges in the entire system. (There is generally no formula that relates N_t to N_e . Two tetrahedra can have 12, 11, or 9 edges depending on whether they have no, 1 or three edges in common. In our discretization, we do not allow two tetrahedra to have touching faces without them being the same.) Similarly, since there are four vertices (nodes) to a tetrahedron, there will also be a large number, say N_n , of nodes in the system.

To each edge in the system is associated a unique Whitney function. If $\mathbf{e} = (\mathbf{v}_1, \mathbf{v}_2)$ denotes an edge in the system joining the node \mathbf{v}_1 to the node \mathbf{v}_2 , then the vector-valued Whitney function \mathbf{W}_e associated to the edge $\mathbf{e} = (\mathbf{v}_1, \mathbf{v}_2)$ is defined by

$$\mathbf{W}_e(\mathbf{r}) = \lambda_{\mathbf{v}_1}(\mathbf{r}) \nabla \lambda_{\mathbf{v}_2}(\mathbf{r}) - \lambda_{\mathbf{v}_2}(\mathbf{r}) \nabla \lambda_{\mathbf{v}_1}(\mathbf{r})$$

where $\lambda_{\mathbf{v}_i}(\mathbf{r})$ is the barycentric function associated to the node \mathbf{v}_i , ($i = 1, 2$), and is the "simplest" piecewise linear function such that $\lambda_{\mathbf{v}_i}(\mathbf{v}_j) = \delta_i^j$, $j = 1, \dots, N_n$. In particular, if \mathbf{v}_i , ($i = 1, \dots, 4$) represent the four vertices of a tetrahedron T , then $\lambda_{\mathbf{v}_i}$ has the following simple representation in T :

$$\lambda_{\mathbf{v}_i}^T(\mathbf{r}) = \mathbf{e}_i \cdot \mathbf{X}^{-1} \begin{bmatrix} \mathbf{r} \\ 1 \end{bmatrix} \stackrel{def}{=} \mathbf{b}_i^T \cdot \mathbf{r} + a_i^T \quad (30)$$

where

$$\mathbf{X} = \begin{pmatrix} \mathbf{v}_1 & \mathbf{v}_2 & \mathbf{v}_3 & \mathbf{v}_4 \\ 1 & 1 & 1 & 1 \end{pmatrix}$$

and

$$\mathbf{e}_i = [\delta_1^i, \delta_2^i, \delta_3^i, \delta_4^i]$$

Furthermore, if $\mathbf{e} = (\mathbf{v}_1, \mathbf{v}_2)$ in an edge of T , a representation of \mathbf{W}_e in T is of the form (using notations in Equation (30)):

$$\mathbf{W}_e^T(\mathbf{r}) = \mathbf{a}_{1,2}^T + \mathbf{b}_{1,2}^T \times \mathbf{r} \quad (31)$$

where

$$\mathbf{a}_{1,2}^T = a_1^T \mathbf{b}_2^T - a_2^T \mathbf{b}_1^T$$

and

$$\mathbf{b}_{1,2}^T = \mathbf{b}_1^T \times \mathbf{b}_2^T$$

With some algebraic manipulations, one can also show that

$$\begin{aligned} \mathbf{a}_{1,2}^T &= \frac{\mathbf{v}_3 \times \mathbf{v}_4}{\det(\mathbf{X})} \\ \mathbf{b}_{1,2}^T &= \frac{\mathbf{v}_4 - \mathbf{v}_3}{\det(\mathbf{X})} \end{aligned}$$

where $\det(\mathbf{X}) = (\mathbf{v}_2 - \mathbf{v}_1) \cdot [(\mathbf{v}_3 - \mathbf{v}_1) \times (\mathbf{v}_4 - \mathbf{v}_1)]$ is the determinant of \mathbf{X} . Hence, the Whitney function associated with the edge $\mathbf{e} = (\mathbf{v}_1, \mathbf{v}_2)$ has a rather simple representation in the tetrahedron T whose vertices are $\mathbf{v}_1, \mathbf{v}_2, \mathbf{v}_3$, and \mathbf{v}_4 :

$$\mathbf{W}_e^T(\mathbf{r}) = \frac{1}{\det(\mathbf{X})} (\mathbf{v}_3 \times \mathbf{v}_4 + (\mathbf{v}_4 - \mathbf{v}_3) \times \mathbf{r}) \quad (32)$$

$$= \frac{(\mathbf{v}_3 - \mathbf{r}) \times (\mathbf{v}_4 - \mathbf{r})}{\det(\mathbf{X})} \quad (33)$$

It should be noted that while $\mathbf{a}_{1,2}^T, \mathbf{b}_{1,2}^T$ and therefore \mathbf{W}_e^T depend on all four vertices $\mathbf{v}_1, \dots, \mathbf{v}_4$ of T , they are invariant, as they should, under the ordering of \mathbf{v}_3 and \mathbf{v}_4 .

The following properties of \mathbf{W}_e are especially relevant to our numerical method. Firstly, the \mathbf{W}_e is divergence-free, i.e., $\nabla \cdot \mathbf{W}_e^T = 0$ for any $\mathbf{r} \in T$. This follows directly from Equation (31).

Secondly, it can be shown algebraically that the tangential component of \mathbf{W}_e^T on each of the two faces of T containing the edge e is dependent only on the vertices making up that face, and, on the other two faces, the tangent component of \mathbf{W}_e^T is identically zero. Since \mathbf{W}_e vanishes identically on any tetrahedron not containing the edge e , the tangential component of \mathbf{W}_e is continuous across all faces of the tetrahedron.

Evaluation of \mathbf{U}_n

To evaluate the integral in Equation (29), we re-write it as follows:

$$\begin{aligned} \mathbf{U}_n(\mathbf{r}) &= \text{PV} \int_V \bar{\mathbf{G}}(\mathbf{r}, \mathbf{r}') \cdot [\tau_1(\mathbf{r}') \mathbf{f}_n(\mathbf{r}')] d\mathbf{r}' \\ &= \mathbf{I}_1^n(\mathbf{r}) + \mathbf{I}_2^n(\mathbf{r}) \end{aligned}$$

where

$$\begin{aligned} \mathbf{I}_1^n(\mathbf{r}) &= \int_{V-V_T(\mathbf{r})} \bar{\mathbf{G}}(\mathbf{r}, \mathbf{r}') \cdot \tau_1(\mathbf{r}') \mathbf{f}_n(\mathbf{r}') d\mathbf{r}' \\ \mathbf{I}_2^n(\mathbf{r}) &= \text{PV} \int_{V_T(\mathbf{r})} \bar{\mathbf{G}}(\mathbf{r}, \mathbf{r}') \cdot \tau_1(\mathbf{r}') \mathbf{f}_n(\mathbf{r}') d\mathbf{r}' \end{aligned}$$

Here $V_T(\mathbf{r})$ is the unique tetrahedron containing \mathbf{r} in its interior. (In the Galerkin's Method, $\mathbf{U}_n(\mathbf{r})$ is eventually multiplied (dot-producted) with the basis functions (Whitney's functions) and integrated numerically over tetrahedra. The second-order numerical integration method employed only requires the evaluation of the dot-product at interior points of tetrahedra.)

The integral in \mathbf{I}_2^n is generally difficult to evaluate over tetrahedra. For this reason, we make the simplifying assumption that

$$\mathbf{I}_2^n(\mathbf{r}) \approx \text{PV} \int_{B(\mathbf{r}, r_{eq})} \bar{\mathbf{G}}(\mathbf{r}, \mathbf{r}') \cdot \tau_1(\mathbf{r}') \mathbf{f}_n(\mathbf{r}') d\mathbf{r}'$$

where $B(\mathbf{r}, r_{eq})$ is a sphere centered at \mathbf{r} with radius r_{eq} given by

$$r_{eq} = \left(\frac{3}{4\pi} \|V_T(\mathbf{r})\| \right)^{\frac{1}{3}}$$

With this radius, the volume of the sphere is exactly the same as the volume of $V_T(\mathbf{r})$, denoted here by $\|V_T(\mathbf{r})\|$. Thus

$$\mathbf{U}_n(\mathbf{r}) \approx \mathbf{I}_1^n(\mathbf{r}) + \text{PV} \int_{B(\mathbf{r}, r_{eq})} \bar{G}(\mathbf{r}, \mathbf{r}') \cdot \tau_1(\mathbf{r}') \mathbf{f}_n(\mathbf{r}') d\mathbf{r}' \quad (34)$$

In many problems, we can reasonably assume the region V is piecewise inhomogeneous. In these cases, we can clearly ensure each tetrahedron is within a region of constant τ_1 . Since the basis functions $\mathbf{f}_n(\mathbf{r}')$ in this study are of the form $\mathbf{a}_n + \mathbf{b}_n \times \mathbf{r}'$, the second integral in Equation (34) can be evaluated explicitly:

$$\begin{aligned} & \text{PV} \int_{B(\mathbf{r}, r_{eq})} \bar{G}(\mathbf{r}, \mathbf{r}') \cdot \tau_1(\mathbf{r}') \mathbf{f}_n(\mathbf{r}') d\mathbf{r}' \\ &= \tau_1(\mathbf{r}) \text{PV} \int_{B(\mathbf{r}, r_{eq})} \bar{G}(\mathbf{r}, \mathbf{r}') \cdot (\mathbf{a}_n + \mathbf{b}_n \times \mathbf{r}') d\mathbf{r}' \\ &= \frac{2\Upsilon(r_{eq})\tau_1(\mathbf{r})}{3k_o^2} (\mathbf{a}_n + \mathbf{b}_n \times \mathbf{r}) \end{aligned}$$

where

$$\Upsilon(r_{eq}) = (1 + j\beta k_o r_{eq}) e^{-j\beta k_o r_{eq}} - 1$$

Results

To test our approach, we calculated the \mathbf{E} field in a homogeneous sphere irradiated by a plane wave and compared the result with the analytic solution (Mie). We did this for several different sets of parameter values and discretizations.

Test Group I.

Our first sets of parameters are those reported in [15]. In particular, we studied two different problems: one is for a transparent sphere in which the conductivity σ is zero and the relative dielectric constant $\epsilon(\mathbf{r})/\epsilon_0$ is identically one, and the other is for a translucent sphere in which $\sigma = 0.015625$ mhos per meter and the relative dielectric constant $\epsilon(\mathbf{r})/\epsilon_0$ is identically 1.015625. In both cases we assume the incident field is a plane wave propagating along the z-axis and polarized in the x-direction. The frequency is taken to be 1000 megahertz and the amplitude is 1 volt per meter. To keep the problem small, we assume the sphere has a 5 cm. radius.

For the assumed frequency, the free space wavelength is approximately 0.3 (m). If we use the commonly quoted rule of thumb of 20 points per wavelength, the mesh size is approximately 0.015 (m) in each of the three directions. A tetrahedron with three sides parallel to the three rectangular coordinate axes and each with length of 0.015 (m) has a volume of 5.625×10^{-7} (m^3), requiring approximately 930 tetrahedra to fill out the given sphere. If we use 10 points per wavelength instead, then the volume of a typical tetrahedron is 4.5×10^{-6} (m^3), requiring approximately 116 tetrahedra to fill out the sphere. To keep our test problem small, we have discretized the sphere using a smaller number of tetrahedra, which in essence amounts to using a smaller number (10 approximately) of points per wavelength. We have designed and implemented two different discretization methods (D1 and D2) for the sphere. Method D1 was used for the transparent case and D2 was used for the translucent case. The major characteristics of the grids resulting from these discretizations are summarized in Table 1.

The discretizations we have chosen for simplicity are relatively coarse, as one can see from the following volume calculation. The volume of our 5 cm-radius sphere is 5.23×10^{-4} (m^3), but the total volume occupied by all the tetrahedra in either the transparent or the translucent case is approximately

$4.0 \times 10^{-4} \text{ (m}^3\text{)}$, which is only 75% of the actual volume. For comparison, the fourth column ("Preferred") in Table 1 shows an example of a discretization using method D2 in which 97.59% of the volume of the sphere was achieved by all the tetrahedra.

Figures 1-9 show graphically the results of these discretizations. As one may see from the plots of the shrunken tetrahedra, the main difference between discretizations D1 and D2 is that the tetrahedra in D2, especially those near the boundary, are more regular (not as flat) than those in D1. Incidentally, the volumes of the tetrahedra in the translucent case have a narrower distribution than that in the transparent case. However, this is not due to the difference in the two methods, but rather to the choice of parameters used to generate these tetrahedra.

The "Preferred" case (Figures 7-9) shows in particular that the discretization method D2 will, in the limit, reproduce the sphere.

Figures 10-11 show the magnitude of the x-component of the total field inside the sphere along the z-axis. They agree quite well with the theoretical results, despite the somewhat coarse discretizations.

Test Group II.

To test the convergence of our method, we refined the discretization for the translucent case further. Figure 12 shows the result of using 288 tetrahedra. This result was unexpected, as it is clearly not as good as that of using 120 tetrahedra (Figure 11). We also tried using 400 tetrahedra, the result (not shown) did not get better. We suspect this non-convergence may have to do with our handling of the singularity of the dyadic Green's function.

We also tested the sensitivity of our method to parameters of the model. Figure 13 shows the result of using a relative dielectric constant of 2.015625 (one unit more than what was used to produce Figure 11.) While this result is apparently not as good as that shown in Figure 11, it is not unreasonable, considering the gross discretization and the increased discontinuity of dielectric constant (between free space and the scatterer.)

Finally, we tested one case in which the frequency was increased from 1 GHz to 10 GHz. The result is shown in Figure 14. Here, the model has consistently under-estimated the actual value, though we can see a mild convergence towards the real solution as the discretization is refined.

Discussion

Our preliminary tests clearly indicate that we should next address the convergence problem. This is likely to involve better handling of the singularity of the dyadic Green's function, as this is the principal approximation used in this method.

TABLE 1. RUN PARAMETERS			
Parameters	Transparent	Translucent	Preferred Grid
Discretization Method	D1	D2	D2
Sphere Radius (m)	0.05 (m)	0.05 (m)	0.05 (m)
No. Tetrahedra	100	120	3648
No. Edges	323	400	11,400
No. Nodes	98	103	3,127
Total Volume (m ³)	4.00×10^{-4}	4.08×10^{-4}	5.11×10^{-4}
Ave Tetra. Vol (m ³)	4.0×10^{-6}	3.4×10^{-6}	1.4×10^{-7}
Min. Tetra Vol (m ³)	1.5×10^{-6}	1.9×10^{-6}	7.4×10^{-8}
Max. Tetra Vol (m ³)	9.0×10^{-6}	6.7×10^{-6}	4.0×10^{-7}
Conductivity, σ (mhos/m)	0.0	0.015625	
Rel. Dielect, (ϵ/ϵ_o)	1.0	1.015625	
Frequency (MHz)	1,000	1,000	
Incident Field			
E_x (volt/m)	1.0	1.0	
E_y (volt/m)	0.0	0.0	
E_z (volt/m)	0.0	0.0	

Conclusion

In this report we describe the progress we have made towards developing a 3D EM interior scattering model to predict energy deposition in realistic biological media. The volume integral approach taken is a natural and mathematically sound method to solve this problem. While we have made much progress, there are obviously several areas that required further analysis. These include

1. Refine singular integral calculations.
2. Upgrade our current method or develop new volume integral equation method to solve our problem.
3. Conduct numerical analysis on the method.
4. Continue validating the model with known solutions and experimental data.

Associated with these analyses is the important question of computational efficiency. Clearly, it is paramount that our model be accurate. However, for a model to become a useful tool, one must be able to apply it to realistic situations. In our case, this means using the model on scatterers of reasonable size (not just small isolated organs). Therefore, in the future, we need to conduct the following closely-related mathematics/computer sciences research:

1. Develop methods to handle larger systems.
2. Explore efficient ways to model pulses.
3. Explore the possibility of using parallel computing to speed up the calculations.

Finally, much research has been and is continued to be done to solve exterior scattering problems due to its obvious military significance. The interior scattering problem that we are interested in, on the other hand, has received relatively little attention. Our emphasis here is to develop a model of interior scattering based on rigorous mathematics to address realistic biological problems (3-dimensional inhomogeneous scatterers). We believe we are heading in the right direction.

References

- [1] Akin, J. E. "Application and Implementation of Finite Element Methods," *Academic Press*, 1982.
- [2] Akin, J. E. "Finite Elements for Analysis and Design," *Academic Press*, 1994.
- [3] Bossavit, A., and Mayergoyz, I. *IEEE Trans. Magn.*, vol. 25, pp. 2816-2821, 1989.
- [4] Chen, Hsing-Yi "Microwave Absorption in Inhomogeneous Models of Man from 500 to 2450 MHz," *J Chinese Institute Engn.*, Vol. 17, pp. 409-414, 1994
- [5] Chen, K. M. and Gurn, B. S. "Internal EM Field and Absorbed Power Denisty in Human Torsos Inudced by 1-500 Mhz EM Waves," *IEEE Trans. Microwave Theory, Tech.*, Vol. 25, pp. 746-755, 1977.
- [6] Chew, W. C. "Waves and Fields in Inhomogeneous Media," *Van Nostrand Reinhold, New York*, 1990.
- [7] Collin, R. E. "Field Theory of Guided Waves," *IEEE Press*, 1991.
- [8] Fikioris, J. G. "Electromagnetic Field Inside a Current Carrying Region," *J. Math. Phys.*, Vol. 6, pp. 1617-1620, 1965.
- [9] Harrington, R. F. "Field Computation by Moment Methods," *Robert E. Krieger Publishing Co.*, 1968.
- [10] Jaroszewicz, T. "Fast Integral Equation Solver for Propagation of Electromagnetic Pulses through Inhomogeneous Irregularly Shaped Dispersive Media," *USAF Armstrong Laboratory Tech. Report MN-94-0008*, 1994.
- [11] Lee, S. W., Boersma, J., Law, C. L., and Deschamps, G. A. "Singularity in Green's Functions and its Numerical Evaluation," *IEEE Trans. Ant. Prop.*, Vol. AP-28, pp. 311-317, 1980.
- [12] Livesay, D. E. and Chen, K. M. "Electromagnetic Fields Induced Inside Arbritrary Sahped Biological Bodies," *IEEE Trans. Microw. Theo. Tech.*, Vol. MTT-22, pp. 1273-1280, 1974.

- [13] Morita, N., Kumagai, N., and Mautz, J. R. "Integral Equation Methods for Electromagnetics," *Artech House, Inc.*, 1991.
- [14] Müller, C. "Foundations of the Mathematical Theory of Electromagnetic Waves," *Springer-Verlag New York*, 1969.
- [15] Penn, J. W. and Cohoon, D. K. "Analysis of a Fortran Program for Computing Electric Field Distributions in Heterogeneous Penetrable Nonmagnetic Bodies of Arbitrary Shape through Application of Tesnor Green's Functions," *USAF School of Aerospace Medicine Tech. Report SAM-TR-40*, 1978.
- [16] Stratton, J. A. "Electromagnetic Theory," *McGraw-Hill, Inc.*, 1941.
- [17] Van Bladel, J. "Electromagnetic Fields," *Hemisphere Publishing Corporation*, 1985.
- [18] Wang, J. J. H., and Papanicolopoulos, C. "Analysis and Measurements of Three-Dimensional Arbitrarily-Shaped Dielectric Scatterers," *RADC-TR-80-167*, Interim Report, May 1980.
- [19] Wang, J. J. H. "A Unified and Consistent View on the Singularity of the Electric Dyadic Green's Functions in the Source Region," *IEEE Trans. Ant. Prop.*, Vol. AP-30, pp. 463-468, 1982.
- [20] Wang, J. J. H. "Generalized Moment Methods in Electromagnetics: Formulation and Computer Solutions of Integral Equations," *John Wiley & Sons, Inc.*, 1991.
- [21] Wandzura, S. "Optimality of Galerkin Method for Scattering Computations", *Microwave and Optical Technology Letters*, Vol. 4, No. 5, April, pp. 199-200, 1991.
- [22] Watson, D. F. "Computing the n-dimensional Delaunay tessellation with application to voronoi polytopes," *The Computer Journal*, vol. 24, pp. 167-171, 1981.
- [23] Whitney, H. "Geometric Integration Theory," *Princeton U.P.*, 1957

- [24] Yuan, X., Lynch, D.R., and Strohbehn, J.W. "Coupling of Finite Element and Moment Methods for Electromagnetic Scattering from Inhomogeneous Objects," *IEEE Trans. Antennas Propagat.*, vol. AP-38, pp. 386-393, March 1990.
- [25] Yuan, X. "Three-Dimensional Electromagnetic Scattering from Inhomogeneous Objects by the Hybrid Moment and Finite Element Method," *IEEE Trans. Microwave Theory Tech.*, vol. 38, pp. 1053-1058, August, 1990.
- [26] Zwamborn, A.P.M., van den Berg, P.M., Mooibroek, J., and Koenis, F.T.C. "Computation of Three-Dimensional Electromagnetic-Field Distributions in Human Body Using the Weak Form of the CGFFT Method," *Appl. Comp. Electromag. Soc. J.*, vol. 7, pp. 26-42, 1992.

Figure 1. Discretization (D1) of a Sphere

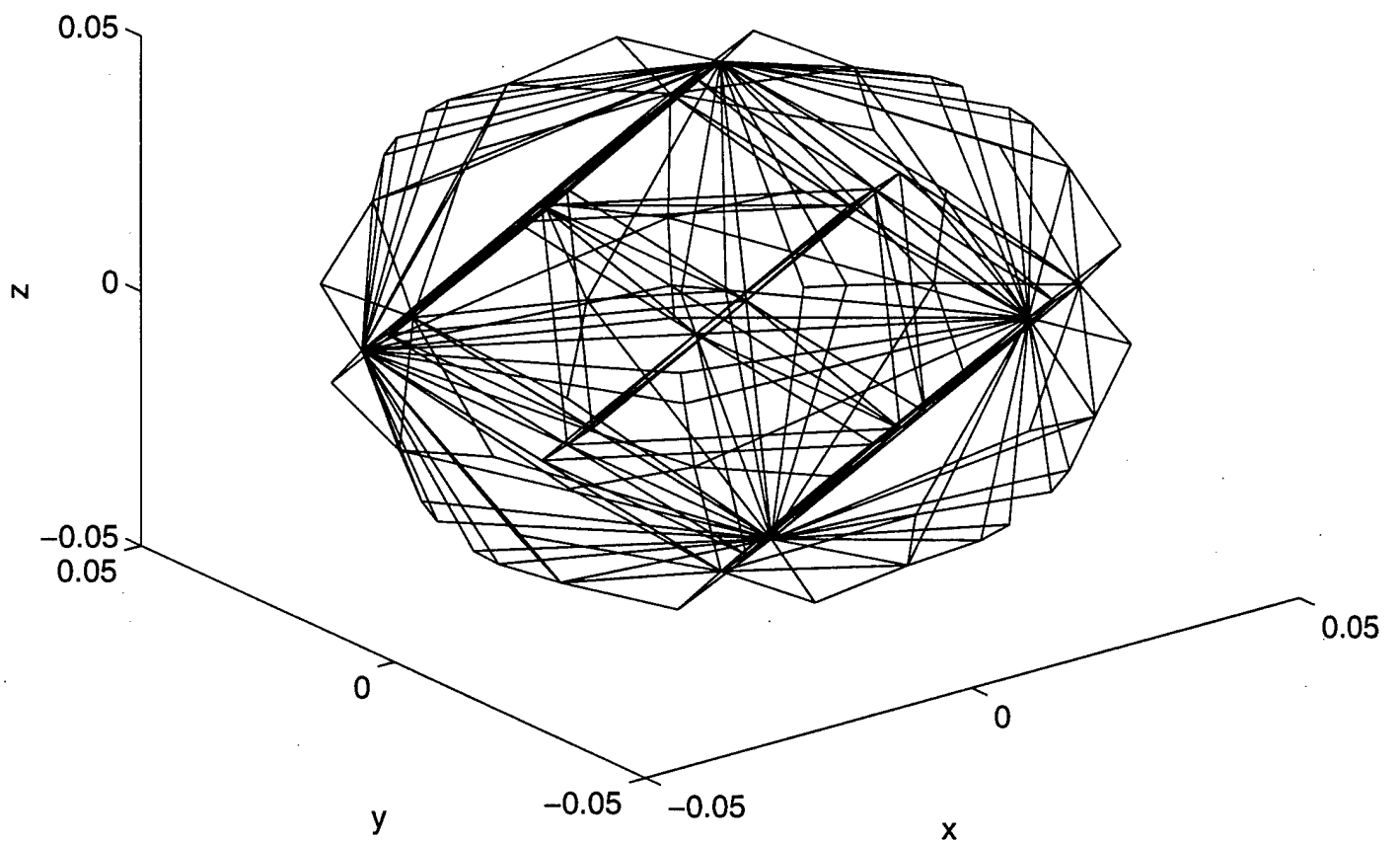


Figure 2. Discretization (D1) of a Sphere (Shrunk)

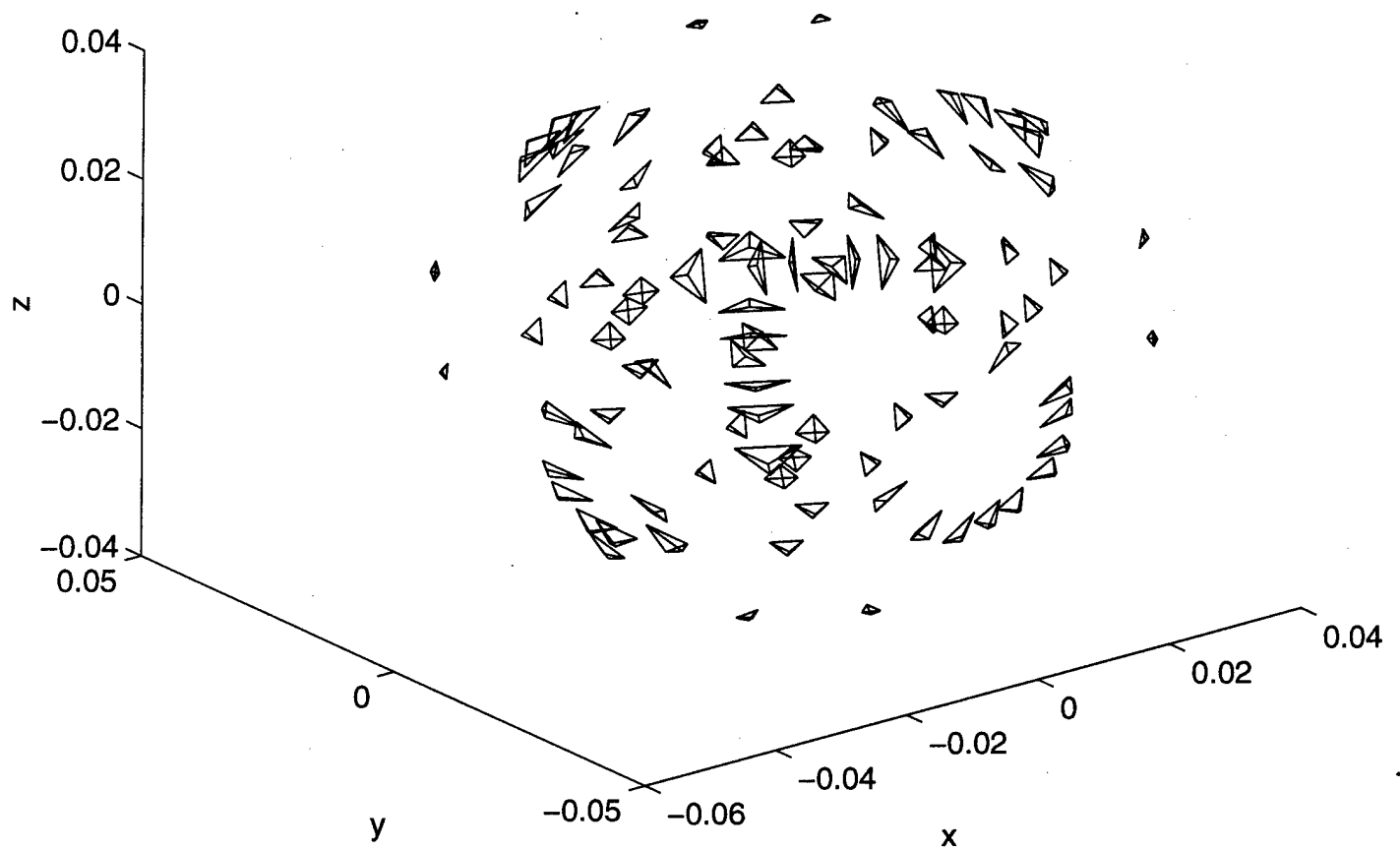


Figure 3. Tetrahedron Volume Distribution (D1)

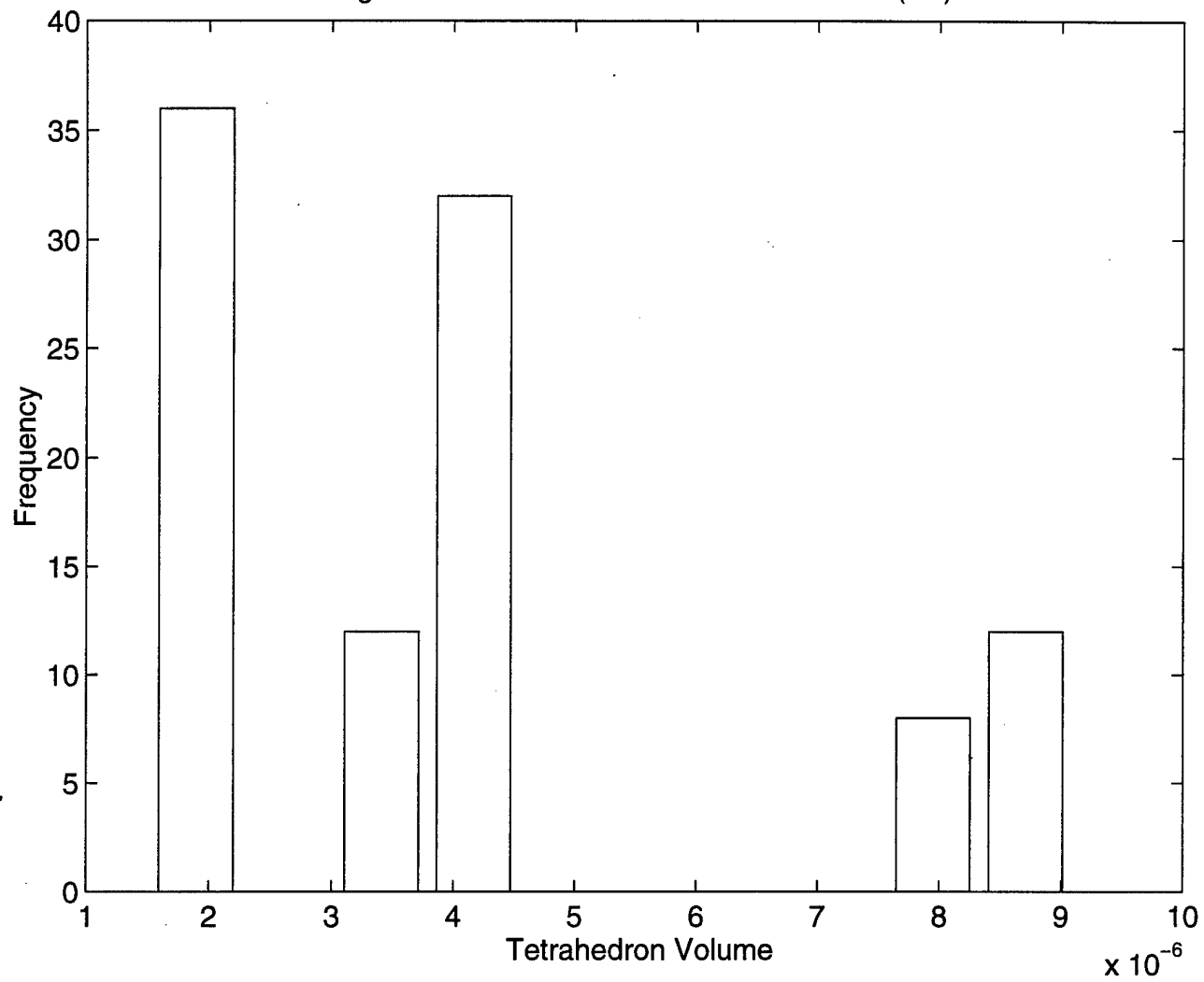


Figure 4. Discretization (D2) of a Sphere

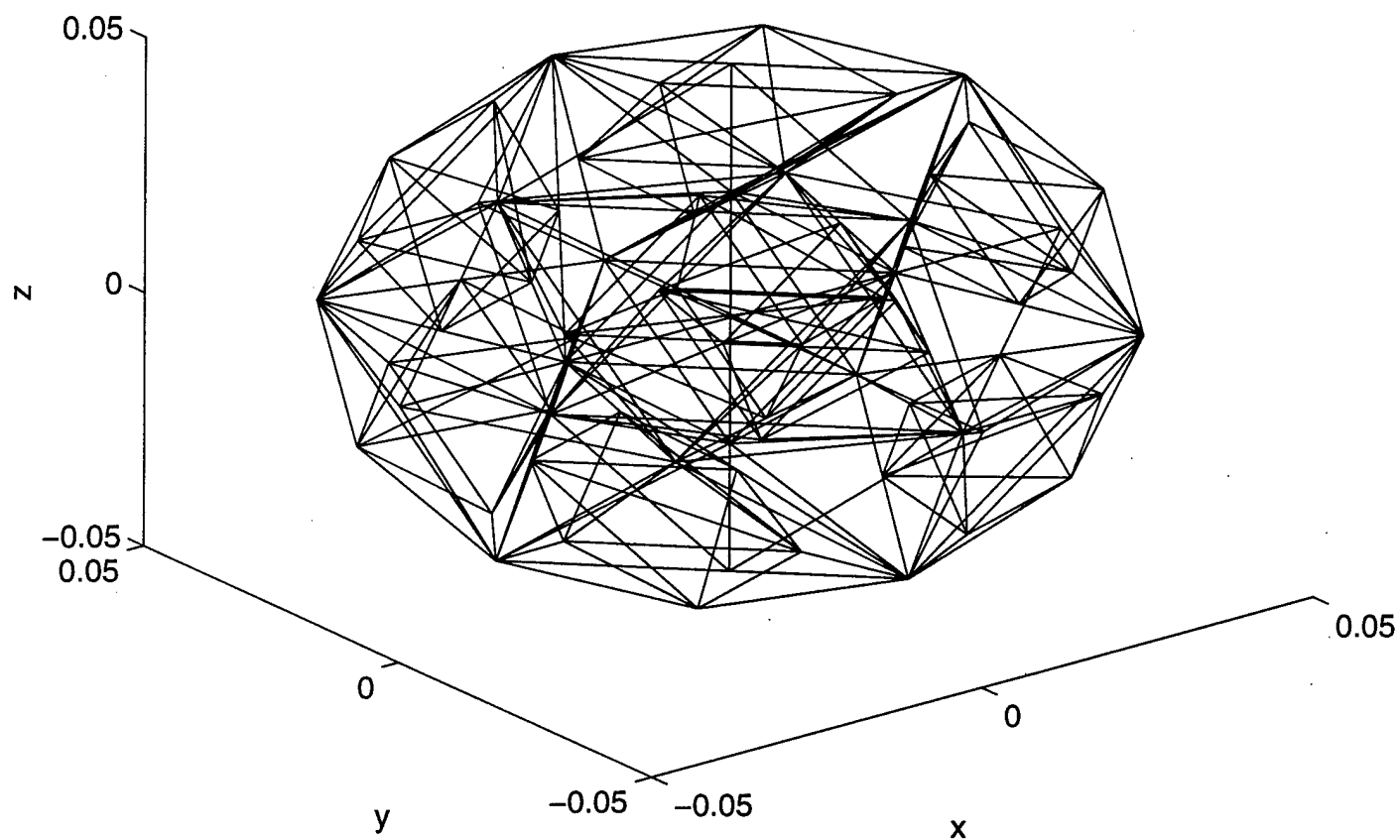


Figure 5. Discretization (D2) of a Sphere (Shrunk)

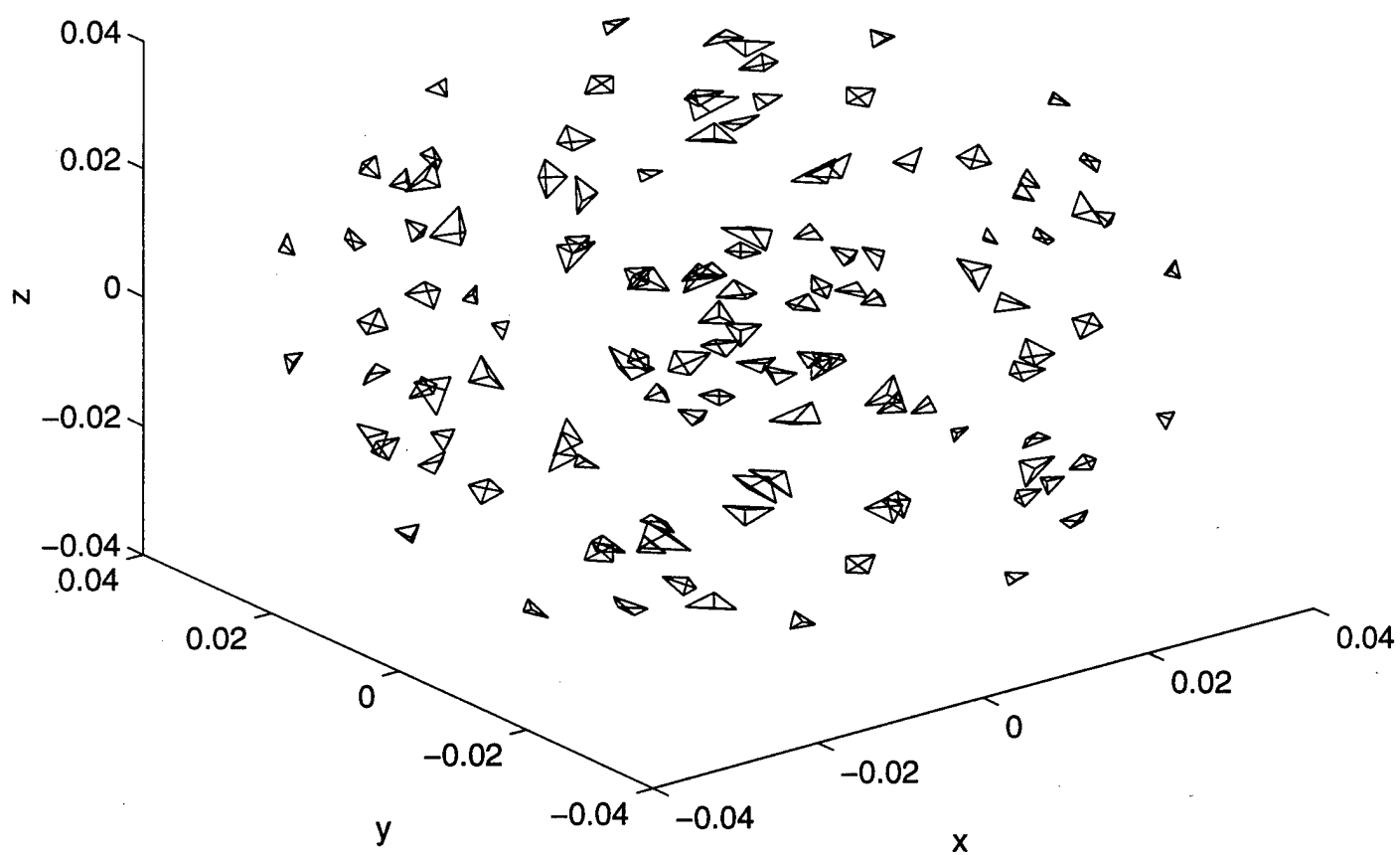


Figure 6. Tetrahedron Volume Distribution (D2)

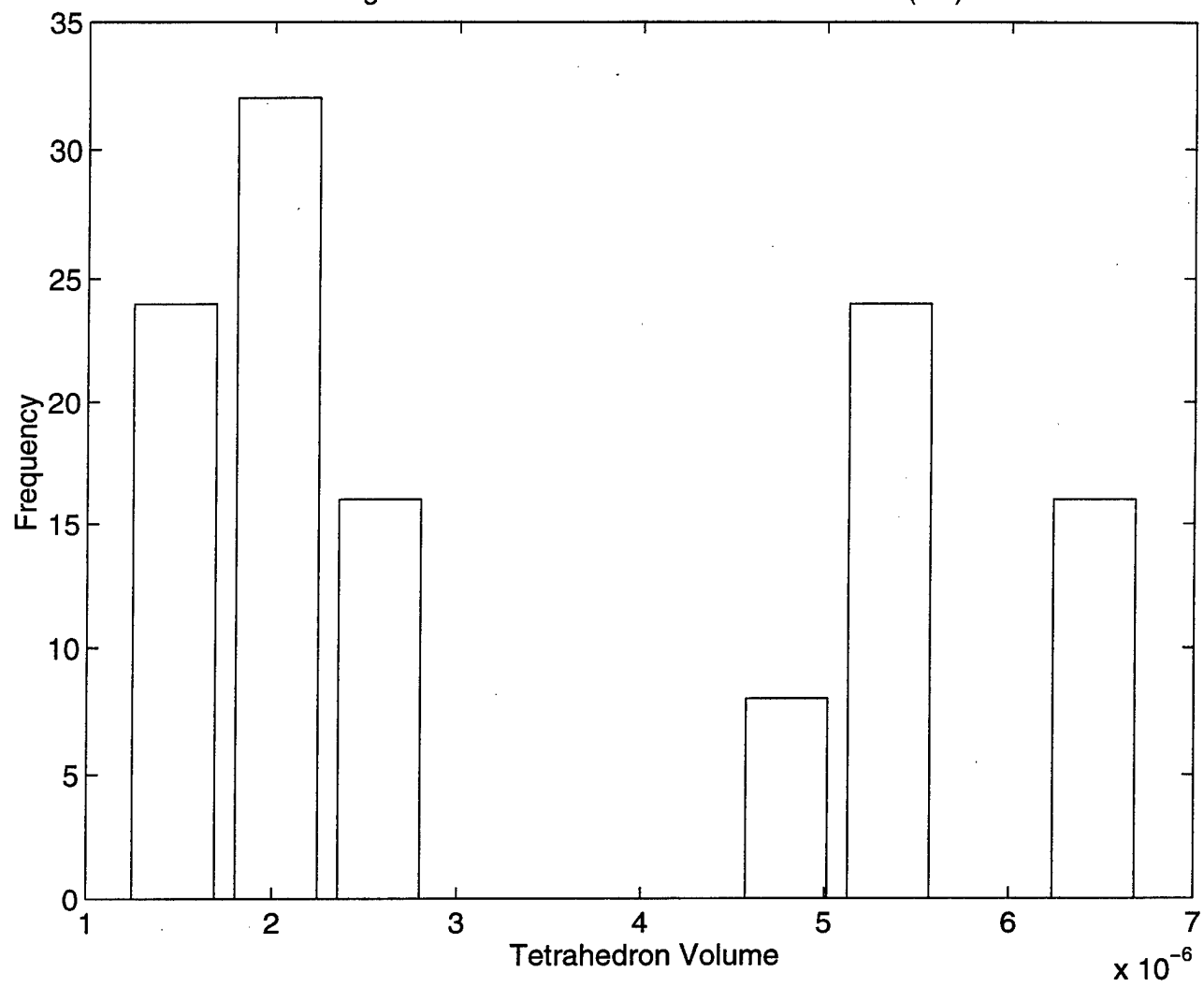


Figure 7. Preferred Discretization of a Sphere

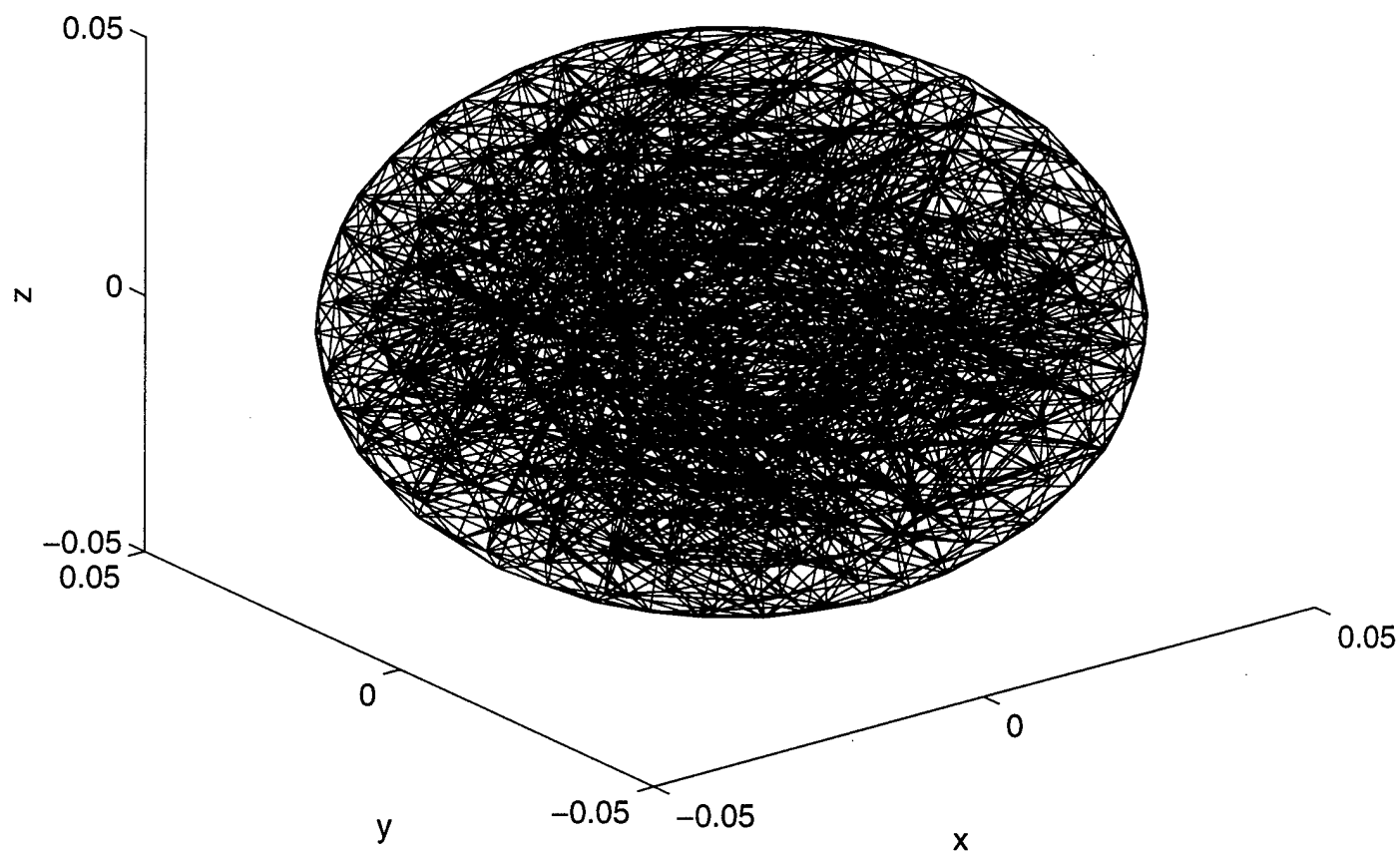


Figure 8. Preferred Discretization of a Sphere (Shrunk)

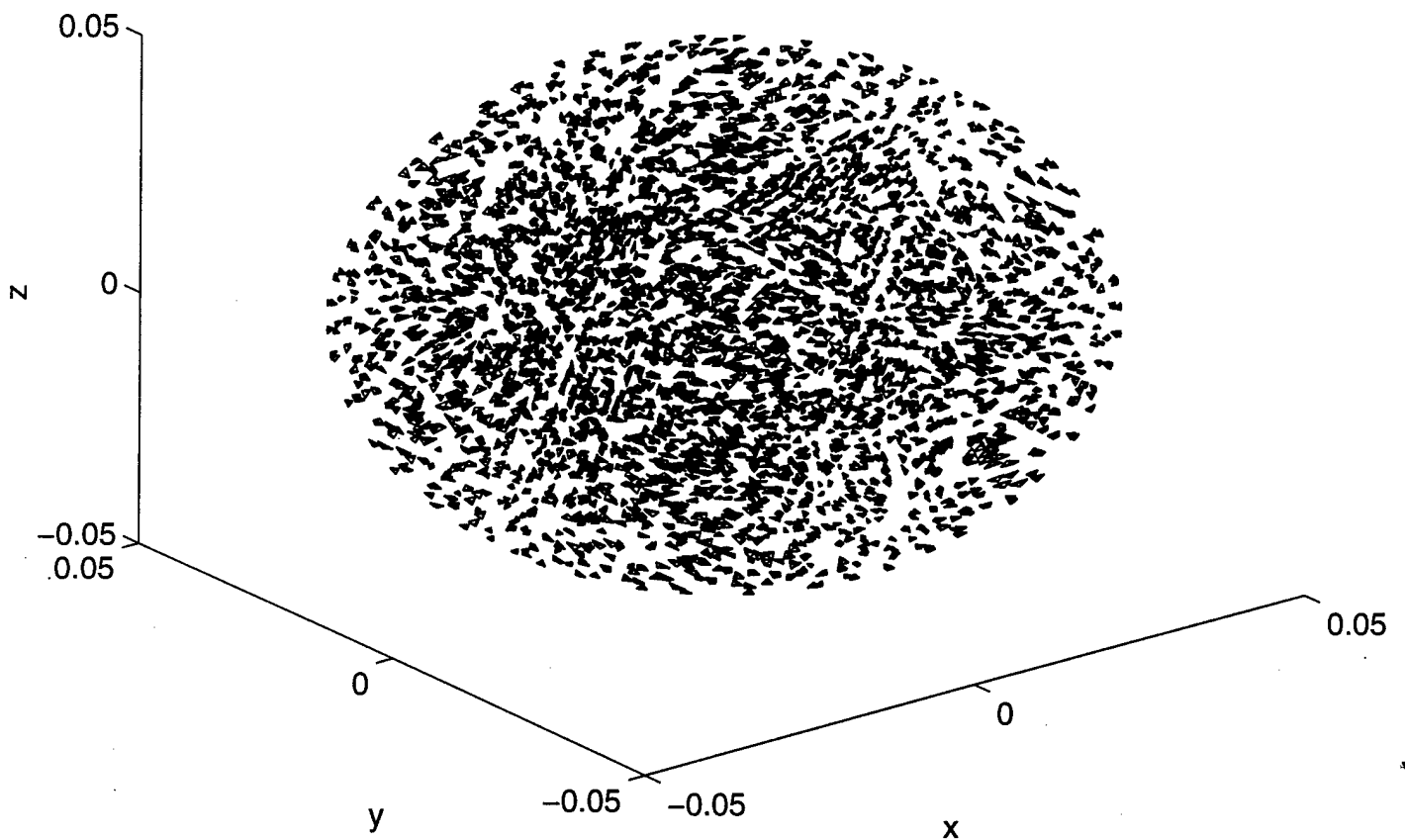


Figure 9. Tetrahedron Volume Distribution (Preferred)

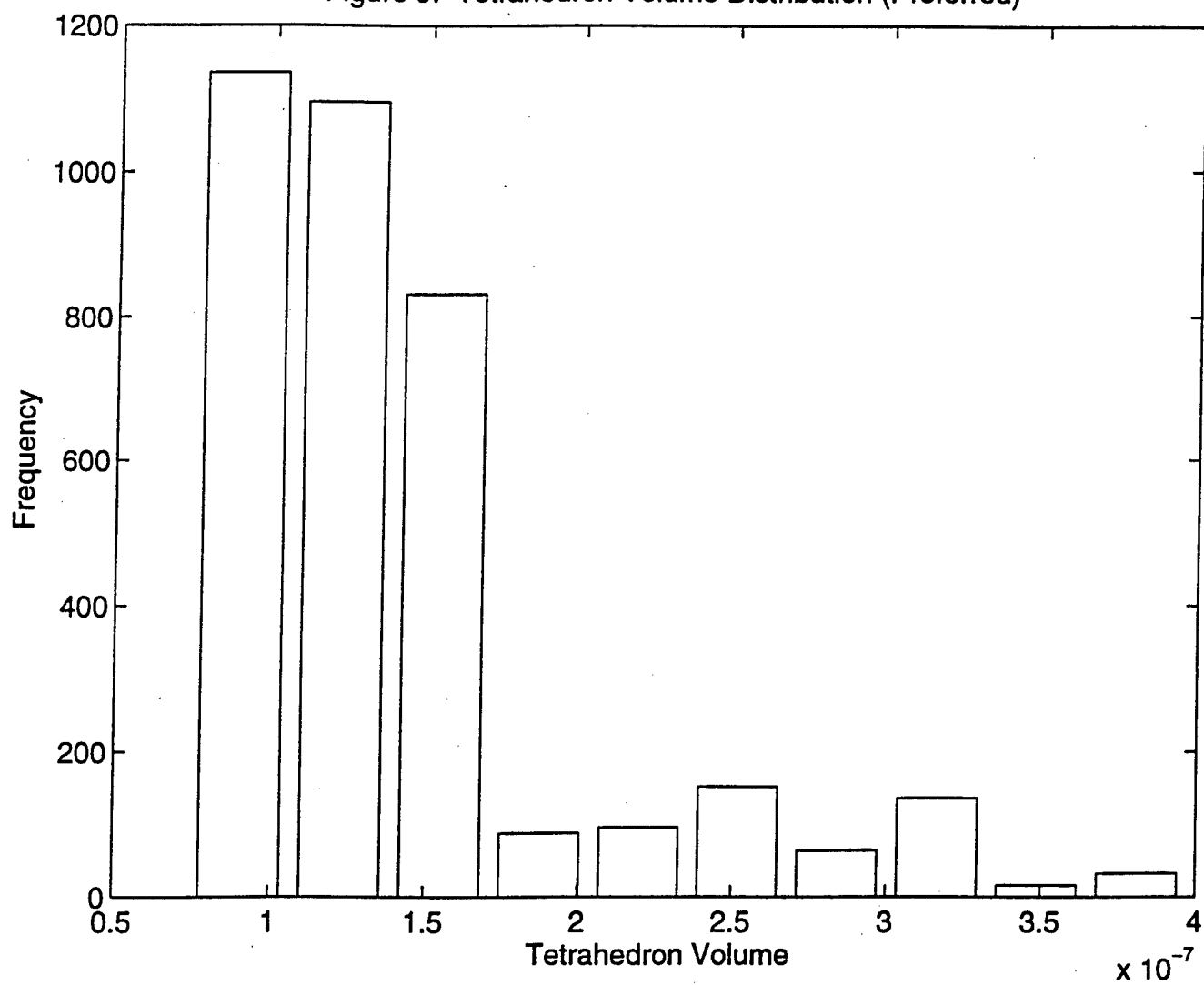


Figure 10. Transparent Case

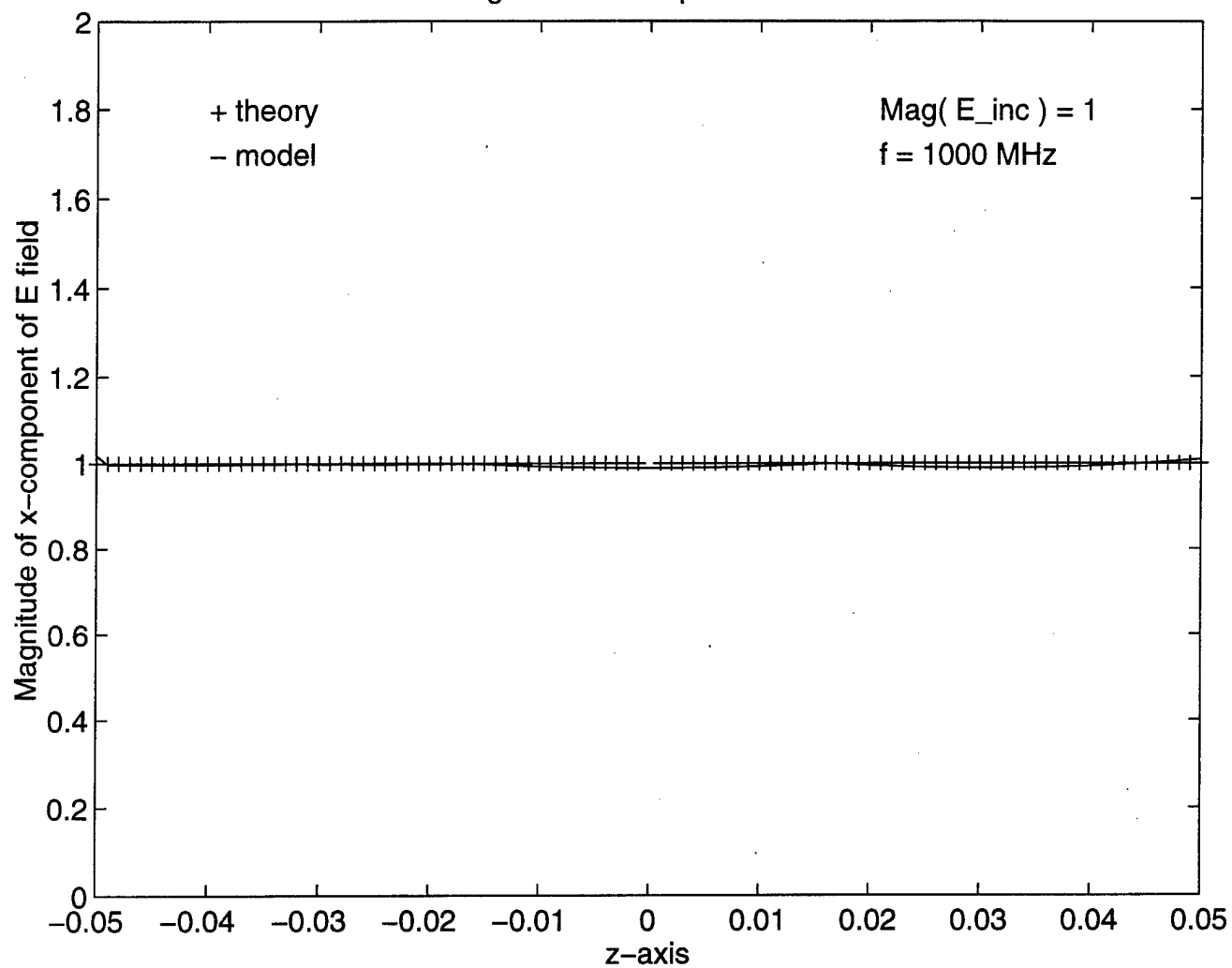


Figure 11. Translucent Case
Magnitude of E_x along z -axis

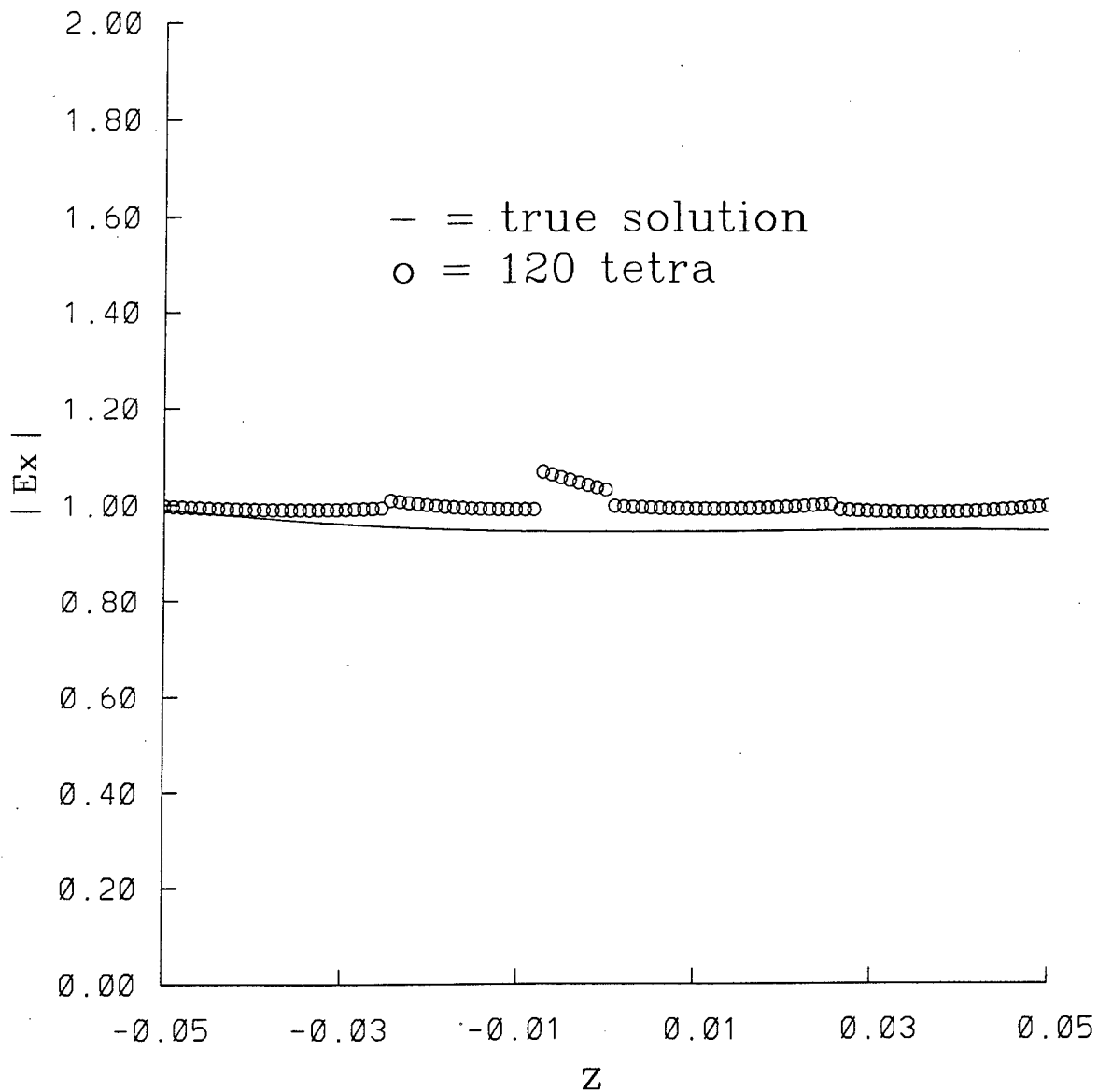


Figure 12. Translucent Case
Magnitude of E_x along z -axis

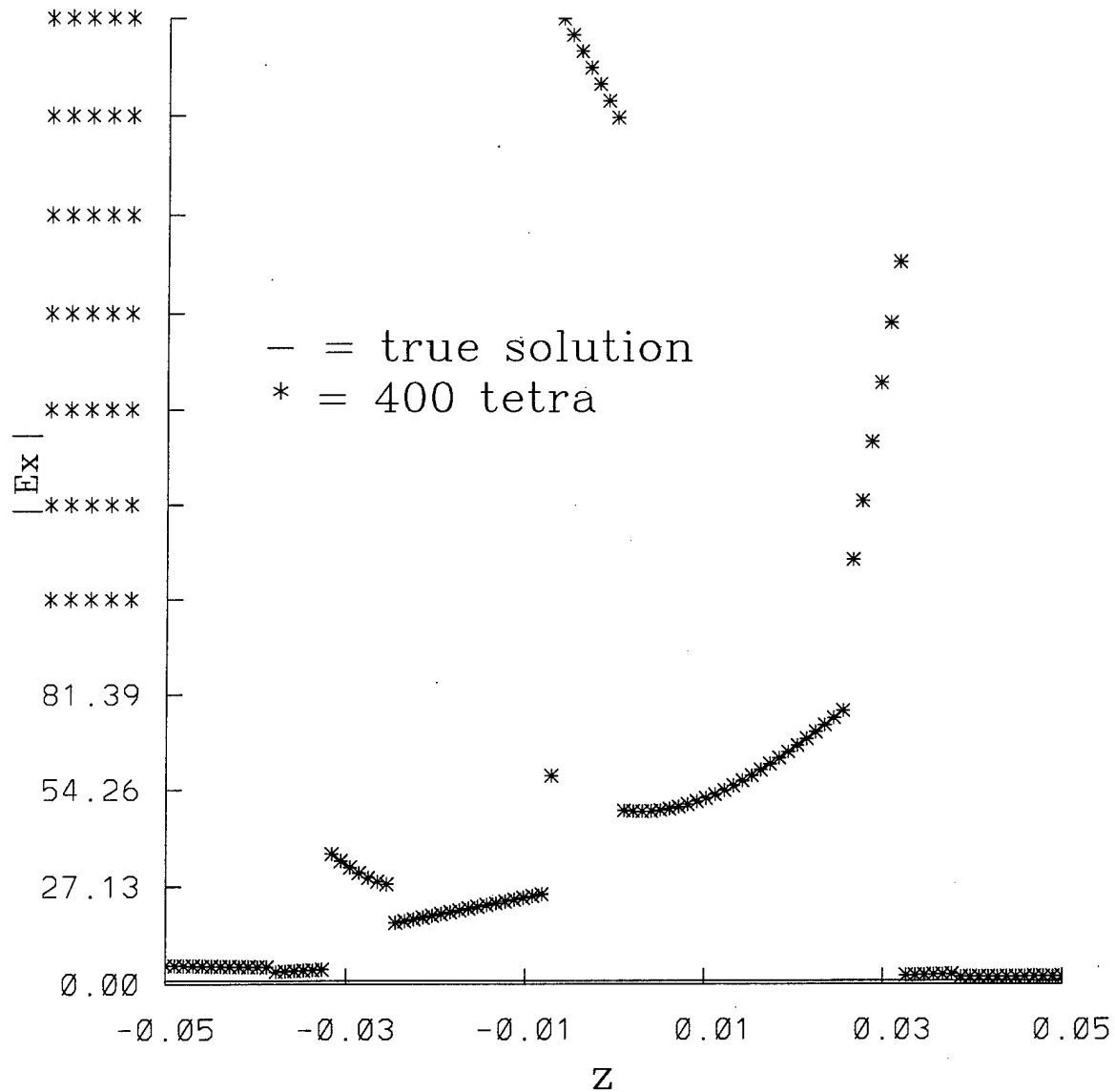


Figure 13. Sensitivity / er
Magnitude of Ex along z-axis

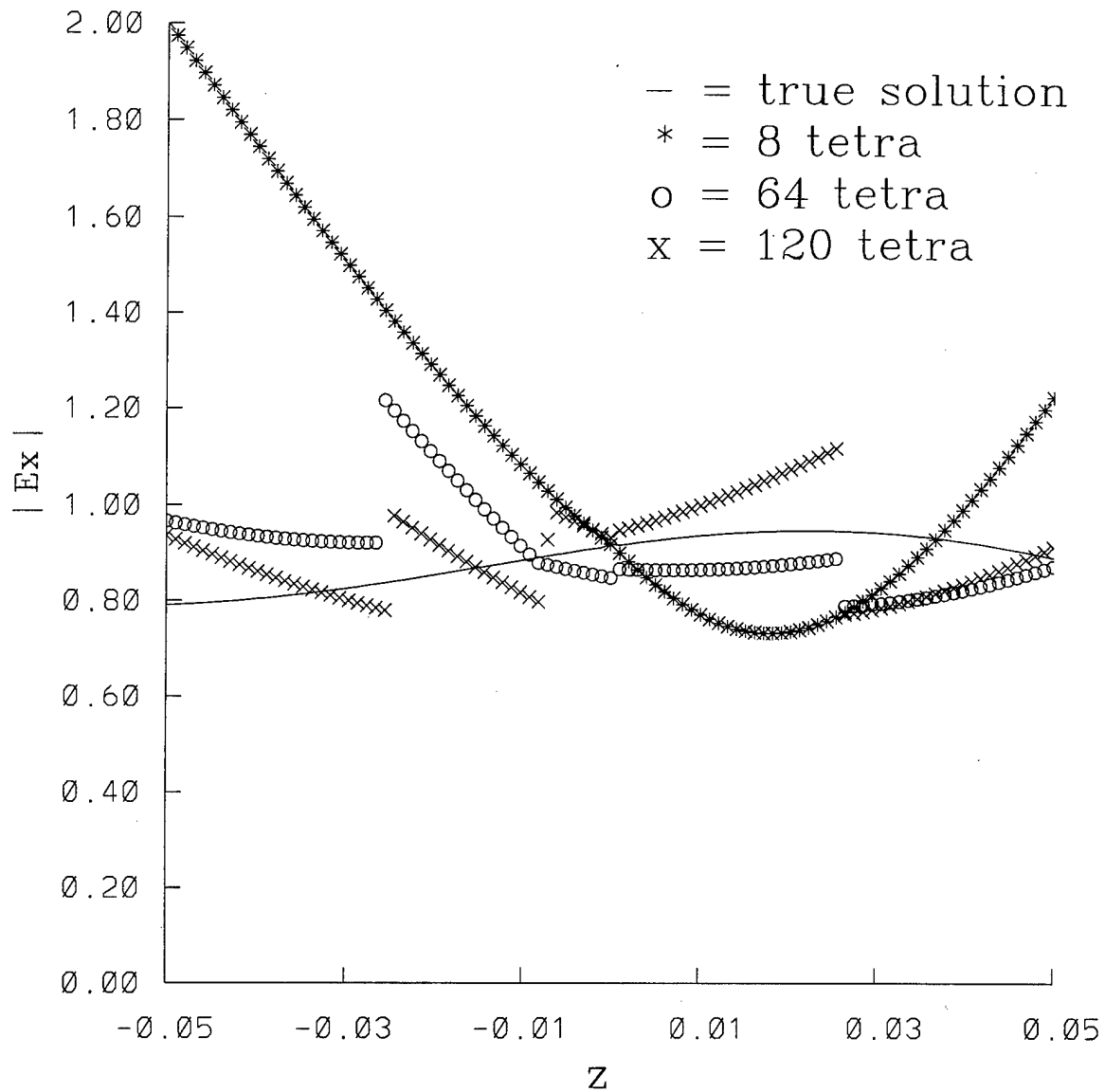


Figure 14. Sensitivity / mhz
Magnitude of E_x along z-axis

